01 Jan 2024

Modified Thermographic Signal-to-Noise Ratio For Active Microwave Thermography

Logan M. Wilcox

Kristen M. Donnell
Missouri University of Science and Technology, kmdgfd@mst.edu

Modified Thermographic Signal-to-Noise Ratio for Active Microwave Thermography

Logan M. Wilcox, *Graduate Student Member, IEEE*, and Kristen M. Donnell, *Senior Member, IEEE*

***Abstract*— Active microwave thermography (AMT) is an active thermographic nondestructive testing and evaluation (NDT&E) technique that uses an active electromagnetic-based excitation. This excitation is achieved through a radiating antenna and is spatially nonuniform in nature. As such, the electromagnetically induced heat is also spatially nonuniform, as it is directly related to the radiated power density incident on the specimen under test (SUT). After excitation, infrared measurements on the surface of the SUT are completed using an infrared camera. Common postprocessing techniques including thermal contrast (*TC*) and signal-to-noise ratio (*SNR*) are often applied to these measured results. As these postprocessing techniques were developed for inspections with a spatially uniform thermal excitation, challenges arise when they are applied to inspections that use a nonuniform thermal excitation. To this end, this work considers two fundamental heating scenarios common in AMT: defect heating and structure heating. Defect heating occurs when the defect is the primary electromagnetic absorber in an SUT, resulting in an induced heat source at the defect location. Structure heating takes place when the surrounding structure of the SUT is the primary electromagnetic absorber (e.g., heat source), and a defect present will affect the thermal diffusion through the SUT. For each scenario, *TC* and *SNR* are calculated. The results indicate that a reformulation of *SNR* is required for structure heating as *SNR* exceeds 0 dB for cases when a defect is and is not present (and hence creates a false positive detection). As such, a new formula is proposed and implemented (SNRSNR_r). The new formula provides a clear indication of the presence of a defect through the calculation of variance over the cooling period (resulting in a difference of SNR_r variance of 9 dB^2 between defect and defect-free specimens). In addition, this new definition is also successfully applied to defect heating (difference of SNR_r variance of 22 dB^2 between cases of with and without a defect).**

***Index Terms*— Active microwave thermography (AMT), defect heating, nonuniform heating, signal-to-noise ratio (*SNR*), structure heating, thermal contrast (*TC*).**

I. Introduction

NONDESTRUCTIVE testing and evaluation (NDT&E) of structures allows for the detection and quantification of defects (i.e., flaws, damage, etc.). NDT&E encompasses many techniques including ultrasound [1], eddy current [2], thermography [3], and microwave [4]. As there are many techniques to choose from, the specific inspection type depends on the inspection need and relative advantages and disadvantages (i.e., remote/noncontact, speed, cost, etc.) of the technique. To this end, a general summary of a few well-known techniques is shown in Table I. As noted in Table I, the properties of the specimen under test (SUT) also play a role when selecting an inspection technique. More specifically, material properties (e.g., electromagnetic, thermal) of the SUT as well as expected defect type, location, orientation, etc. must be considered to ensure that the inspection technique will be capable of successful detection.

TABLE I
ADVANTAGES AND DISADVANTAGES OF NDT TECHNIQUES [1], [2], [3], [4]

NDT&E Technique	Advantages	Disadvantages
Ultrasound	·Widely applicable to many types of material ·One-sided inspection	·Sensitive to SUT geometry ·Usually requires contact
Eddy Current	·Rapid inspection time ·Sensitive to changes in material properties	·Sensitive to defect orientation ·Lift-off distance needs to be minimized
Thermography	·Advanced signal processing techniques ·Quick and large area inspections	·Cannot inspect thermally insulating materials ·Limited image resolution
Microwave	·Detection of subsurface defects ·One-sided inspection	·Cannot inspect electrically conductive materials beyond surface

One technique that has found sustained inspection success in the infrastructure, aerospace, and space industries (amongst others) is thermography. In this approach, heat is generated on and/or within an SUT and the resulting surface thermal profile is measured with an infrared (or thermal) camera. This surface thermal profile is recorded for postprocessing, with the spatial and temporal variations in surface temperature related to information about the structure such as material properties or presence of potential defects.

Generally speaking, thermography is an attractive technique due to its ability to inspect large areas, the straightforward and easy to interpret results, the well-established postprocessing methods, and the option for a passive or active thermal excita-

Manuscript received 11 September 2023; revised 4 December 2023; accepted 17 December 2023. Date of publication 5 January 2024; date of current version 18 January 2024. This work was supported in part by the Kummer Innovation and Entrepreneurship Doctoral Fellowship at Missouri University of Science and Technology, in part by the IEEE Instrumentation and Measurement Society (I^{2}MTC) 2021 Graduate Fellowship Award, and in part by the U.S. Air Force SBIR Topic Entitled "Small Business Innovation Research Program (SBIR)-Phase II: Nondestructive Evaluation of Composite Substrates Below Thick Top Coat Materials" through SBIR Phase II under Grant AF183-041. The Associate Editor coordinating the review process was Dr. Wei Fan. *(Corresponding author: Logan M. Wilcox.)*

The authors are with the Microwave Sensing (μSense) Laboratory, Department of Electrical and Computer Engineering, Missouri University of Science and Technology, Rolla, MO 65409 USA (e-mail: lmwc65@mst.edu; kmdgfd@mst.edu).

Digital Object Identifier 10.1109/TIM.2024.3350148

tion. Passive thermography occurs when the thermal excitation is naturally occurring (i.e., the sun heating a highway). Active thermography occurs when heat is induced on/in an SUT via an external and controlled excitation source [3]. Examples of this include traditional active thermography that uses a flash lamp excitation [3], as well as laser [5], vibration [6], microwave [7], [8], etc. that have become more common in recent years. As it relates to a microwave-based excitation, this approach has become more popular as of late and is often referred to as active microwave thermography (AMT). AMT has found success in numerous civil and aerospace-related applications including defect detection in cement-based [9], rubber [10], and radar absorbing [8], [11] materials, among others.

As an active thermographic technique, AMT uses electromagnetically induced heating. This is accomplished by a radiating antenna (such as a horn or patch antenna) illuminating an SUT with microwave energy (usually on the order of tens of watts). When this energy is incident upon the SUT, some will be reflected by and some transmitted into the SUT. Within this transmitted energy, a portion of it is subsequently absorbed by the SUT and hence transformed to heat. In this way, a thermal excitation is generated.

During an AMT inspection, there are two types of heating scenarios that are considered fundamental within AMT, These scenarios depend on whether the induced heat manifests primarily in the defect itself (referred to as defect heating) or within the material(s) of the SUT (referred to as structure heating). The first scenario, defect heating, occurs when the defect itself has properties such that it absorbs substantially more electromagnetic energy than the surrounding SUT. This heat induced in the defect diffuses through the SUT to the inspection surface where it can be detected as a thermal increase with a thermal camera. The second scenario, structure heating, occurs when the structure itself is the primary absorber of electromagnetic energy and hence serves as the heat source. In this context, structure heating refers to a scenario where any part of an SUT (other than the defect) volumetrically absorbs the incident microwave energy and hence is considered the primary volumetric heat source. In such cases, a change in the temperature on the inspection surface in the area above the defect will manifest.

As the measured results in an AMT inspection are thermographic in nature, established thermographic postprocessing techniques may also be applied to AMT inspection results. These techniques were developed under the assumption that uniform heating occurs throughout the inspection (as is the case for the traditional flash lamp excitation [12]). However, as the thermal source in an AMT inspection is initially electromagnetic in nature (i.e., electromagnetic energy radiated from an antenna), the induced heat is directly proportional to the radiated energy. As such, the spatial distribution of the induced heat over an inspection surface is directly related to the spatial distribution of the impinging electromagnetic energy (e.g., the power density) over the same. To this end, the traditional thermographic postprocessing techniques must be reexamined for applicability to nonuniform heating (as is the case for AMT) for the two fundamental types of heating scenarios mentioned above (defect and structure heating) relevant to AMT.

II. Background

As mentioned previously, AMT uses microwave-induced heating for the thermal excitation. Physically speaking, this is accomplished through dielectric/magnetic absorption of the microwave energy (by the SUT) that is incident upon the same. This absorption is directly related to the dielectric and magnetic properties of the SUT which, when referenced to free space, are denoted as $\varepsilon_r = \varepsilon_r' - j\varepsilon_r''$ and $\mu_r = \mu_r' - j\mu_r''$, respectively. Here, ε_r' and μ_r' are the relative permittivity and permeability, respectively, which represent the ability of the SUT to store (electric/magnetic) energy. In addition, and of more interest to AMT, ε_r'' and μ_r'' are the dielectric and magnetic loss factors, respectively. These quantities represent the ability of the SUT to absorb electric/magnetic energy, which in turn facilitates heat generation, Q (J), as [13]

$$Q = 2\pi f\left(\varepsilon_0\varepsilon_r''|E|^2 + \mu_0\mu_r''|H|^2\right) \tag{1}$$

where f is the frequency (Hz) of the incident electromagnetic energy, ε_0 (F/m) is the permittivity of free space, μ_0 (H/m) is the permeability of free space, E is the complex incident electric field (V/m), and H is the complex incident magnetic field (A/m). This heat source causes a spatially varying surface thermal profile (the measured quantity of interest for an AMT inspection), T (K). To this end, the relationship between Q and T is shown as [14]

$$\left(\frac{\partial}{\partial t} - \alpha\nabla^2\right)T = \frac{1}{\rho c}Q \tag{2}$$

where α is the thermal diffusivity (mm^2/s), ρ is the density (kg/mm^3), c is the specific heat (J/(kg·K)), t is time (s), and ∇^2 is the Laplacian operator (divergence of the gradient of a scalar function).

Two postprocessing techniques commonly used in traditional thermography that have also been applied in AMT are *TC* and signal-to-noise ratio (*SNR*) [9]. These techniques consider the thermal response of region(s) where a suspected defect exists along with that of a known sound (or defect-free) location. *TC* is defined as

$$TC(t) = [T_D(t) - T_{aD}] - [T_S(t) - T_{aS}] \tag{3}$$

where $T_D\ (K)$ is the temperature at the defect location, $T_S\ (K)$ is the temperature at a given sound location, $T_{aD}\ (K)$ is the ambient temperature at the defect location (i.e., at $t = 0$, the start of the inspection), and $T_{aS}\ (K)$ is the ambient temperature at the same sound location (again, at $t = 0$). *TC* includes a reference to ambient temperature as it has been found that an approach that considers a temperature increase (i.e., with respect to ambient) versus absolute temperature is preferred to remove dependency on (variable) ambient conditions [9]. In the past, *TC* has been applied to AMT inspection results to increase the visual clarity of a defect within a thermal image and quantify the difference in temperature when a defect is present (versus a defect-free scenario) [8], [9]. However,

in a practical setting, using *TC* requires a known defect-free location or access to a separate defect-free SUT (of properties identical to the test specimen) for reference measurement. This renders the use of *TC* impractical for realistic inspection scenarios.

The other parameter that incorporates the measured T of (2) is *SNR*. *SNR* represents the thermal variation over an inspection surface (cross section of the SUT) with respect to a sound location (specified/finite area on an inspection surface) and is defined as [15]

$$SNR(t) = 20\log_{10}\frac{|\mu_D(t) - \mu_S(t)|}{\sigma_S(t)} \tag{4}$$

where μ_D (K) is the mean surface temperature at the defect location, μ_S (K) is the mean surface temperature in the sound location, and σ_S (K) is the standard deviation of the temperature in the sound location. The quantities μ_D, μ_S, and σ_S are calculated from the following:

$$\mu_{D,S}(t) = \frac{1}{N_p}\sum_{p=1}^{N_p}\Delta T_p(t) \tag{5}$$

$$\sigma_S(t) = \sqrt{\frac{1}{N_p}\sum_{p=1}^{N_p}\left[\Delta T_p(t) - \mu_S(t)\right]} \tag{6}$$

where ΔT_p (K) is the temperature (with respect to ambient temperature) at a given pixel, p, in a specified location (defect or sound), and N_p is the number of pixels (in the thermal image). As it relates to defect detectability, when *SNR* exceeds 0, a defect is considered detectable [18]. Previously, *SNR* [9] has been used to reduce the impact of noise on results (i.e., environmental, infrared camera, structural heating, etc.) during an AMT inspection. However, as AMT uses a nonuniform thermal excitation, this work considers the current definitions of *TC* (3) and *SNR* (4) in the context of nonuniform excitation and proposes a new definition of *SNR* that is better suited for inspections that feature nonuniform structural heating. The existing definition of *SNR* (and the proposed modified *SNR*) are specifically for temperature. This is important to note as there is also a definition of *SNR* that is calculated based on the phase of an infrared image [16] (obtained via thermographic analysis in the frequency domain). This stems from the thermographic postprocessing technique of pulse phase thermography (PPT). PPT is used to analysis thermographic data in the frequency domain through amplitude and phase of the measured data [17]. In addition, PPT can be used to generate phase contrast images that may provide information about defect depth and size. Such an analysis may also advance the capabilities of AMT as it relates to defect quantification. However, before AMT can be expanded to include PPT, the significant thermal nonuniformity resulting from the microwave illumination across the inspection area of interest must first be addressed. To this end, in this work, a modified definition of *SNR* is presented that is independent of thermal excitation uniformity. *SNR* was specifically selected for modification due to its inherent sensitivity to the presence of a defect (which, in its current definition, is not accurate for certain AMT inspection scenarios).

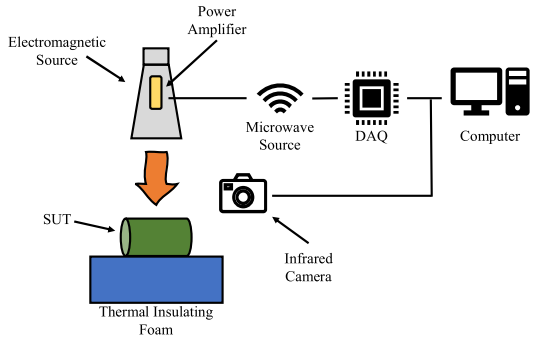

Fig. 1. Illustrative view of an AMT system.

III. AMT Inspection Process

The AMT system used in this work comprises a 50-W power amplifier, a data acquisition unit (DAQ), microwave source, computer, ridged pyramidal horn, and infrared camera (FLIR T430sc with a thermal sensitivity of 30 mK). In addition, thermal insulting foam is placed behind the SUT to create an adiabatic boundary (i.e., no heat transfer past the backside of the SUT). This was not necessary on the sides of the SUT as the heat is primarily located in the center of the inspection surface of the SUT and is minimal (approaches zero) on the sides. This was done so no heat transfer occurred on the largest surface that is not the inspection surface. An illustrative representation of the system can be seen in Fig. 1. For all the measurements reported in this work using the setup of Fig. 1, the antenna is centered directly over the defect.

As mentioned previously, a ridged pyramidal horn antenna with physical aperture dimensions of 23 × 17 cm is used in this work to illuminate the SUT with electromagnetic energy. To illustrate the nonuniform power density radiated by this antenna, a simulation was conducted using CST Microwave Studio.[1] The simulation considers an electromagnetically absorbing material (30.5 cm × 30.5 cm× 0.2 cm with $\varepsilon_r = 2 - j3$ and $\mu_r = 5 - j10$) under 50 W of electromagnetic illumination at a frequency of 2.4 GHz (operating frequency for this work). The lift-off distance (i.e., distance between the aperture of the antenna and the inspection surface) is 30 cm. The simulated power density and resultant thermal surface profile over the inspection surface can be seen in Fig. 2. The thermal surface profile was calculated after 1 s of illumination (to minimize the effect of thermal diffusion that would need to be considered if a longer excitation was used).

As can be seen in Fig. 2, the resultant thermal surface profile is spatially similar to that of the power density and therefore is nonuniform. As noted previously, this nonuniform thermal distribution that occurs during AMT inspections may limit the applicability of the traditional postprocessing techniques (i.e., *TC* and *SNR*), as these techniques were developed for a more uniform thermal excitation. More specifically, in traditional thermography, since the thermal excitation is

[1]Registered trademark.

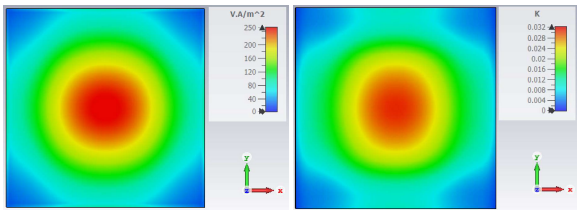

(a) (b)

Fig. 2. (a) Simulated power density and (b) resultant thermal surface profile.

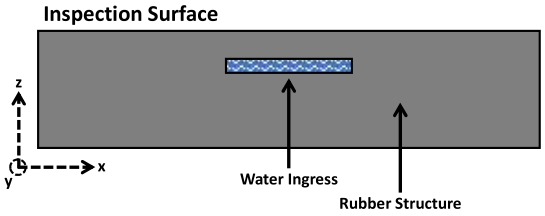

Fig. 3. Illustrative view of a rubber structure undergoing water ingress.

uniform (due to the flash lamp heat source), the sound location measurement needed for computation of *TC* and *SNR* may be selected arbitrarily since all the sound locations have, effectively, the same average temperature and standard deviation. However, for a nonuniform thermal excitation (as is the case for AMT), the selection of a sound location may have a substantial impact on postprocessing since the thermal excitation varies spatially over the inspection surface. As such, the temperature statistics (average, μ, and standard deviation, σ) of the sound location also vary spatially over the inspection surface (as per the spatial incident power density) and hence, the calculated *TC* and *SNR* will depend on the same. This is problematic as a spatial dependence of *TC* and *SNR* may affect defect detection outcomes (e.g., false positive and/or negative).

To illustrate the impact of nonuniform excitation on (3) and (4), the two previously mentioned fundamental AMT heating scenarios are considered. The first is defect heating, where the surrounding structure undergoes a minimal thermal increase during inspection. An example of this can be seen when a low-loss rubber structure undergoes water ingress. Here, the water ingress heats, and this heat diffuses through the rubber structure to the inspection surface. The second is structure heating, where the structure itself experiences a majority of the thermal increase and defects present instead affecting the flow of heat. An example of this is an absorbing topcoat on a carbon-fiber-reinforced polymer (CFRP) substructure that has undergone impact damage. Here the topcoat heats and the presence of the damaged area increases the surface temperature over the defect (as thermal properties are affected by the damage). Again, and as mentioned, structure heating in this context refers to when any part of the SUT is the primary heat source of AMT inspection.

A. Scenario 1: Defect Heating

As mentioned previously, one heating scenario for AMT is referred to as defect heating. In this case, when a lossless or low-loss structure containing a defect with a greater loss factor than the surrounding material is illuminated with microwave energy, the defect itself will heat more significantly than the structure. An example of this type of heating where AMT has found success in defect detection is when a low-loss rubber structure suffers from water ingress, as is illustratively shown in Fig. 3.

Measurements were completed on such an SUT using the AMT system illustrated in Fig. 1. The rubber structure has a cross section of 30.5 cm $\times$ 30.5 cm and a thickness of 2 cm. The dielectric properties of the rubber were measured as $\varepsilon_r = 5.02 - j0.05$ (measured at the *R*-band (1.72–2.6 GHz) using the open-ended waveguide technique with a modified flange as per [19]). Here, the low-loss nature of the structure (rubber) is clear with a relative loss factor of 0.05. The operating frequency for this measurement was selected to be 2.4 GHz because, at this frequency, water has a high loss factor ($\varepsilon_r = 77 - j9$ [20]). In addition, since the rubber is low loss, it will absorb minimal incident energy, and hence minimal surface (and structure) heating will occur during inspection. In other words, the defect will serve as the primary heat source in this case.

To model the effect of the rubber structure undergoing water ingress, a piece of paper towel with a cross section of 4 cm $\times$ 4 cm, thickness of 0.0375 cm, and containing 1 mL of tap water was placed 0.2 cm below the inspection surface, in between two identical layers of rubber. A paper towel was used to contain the water, as it has minimal volume over a relatively large area compared with thickness (i.e., 2-D instead of 3-D) and has low permittivity and loss factor when compared with water. In this way, the presence of the paper towel minimally affects the measurement results (i.e., will not impact the thermal diffusion as the rubber layers are in direct contact everywhere aside from the location of the paper towel). To ensure water did not expand past the intended region (i.e., the paper towel), the region on the rubber SUT where the wet paper towel was placed was measured (on both the layers of rubber) to ensure that the water remained within the intended 4 cm $\times$ 4 cm area. It was observed that the wet footprint left by contact with the paper towel did not extend past the intended region (for both layers).

During AMT inspection, the total inspection time was 600 s, with a 300 s heating period and 300 s cooling period. For comparison, two SUTs were considered, one with a defect (WD) and another without a defect (WOD, identical to WD but without the wet paper towel), with *TC* and *SNR* calculated for both. The sound parameters (μ_S and σ_S) were calculated for several different locations (each a 5 cm $\times$ 5 cm area) on the SUT surface, with a map of the sound measurement locations shown in Fig. 4. These sound locations were arbitrarily selected outside the known location of the defect (denoted yellow in the center of Fig. 4) and were the same for the WD and WOD SUTs. By selecting different sound locations, the effect of the sound parameters (T_S, μ_S, and σ_S) in (4) and (5) on *TC* and *SNR* can be studied. The results for both, calculated per (3) and (4) and per each sound location for the WD and WOD SUTs, can be seen in Figs. 5 and 6, respectively. In addition, Table II shows the maximum and final (i.e., at the

TABLE II
MAXIMUM AND FINAL *TC* FOR WD AND WOD FOR DEFECT HEATING (FIG. 5)

Sound Location	WD		WOD	
	Maximum (K)	Final (K)	Maximum (K)	Final (K)
1	2.49	1.10	0.02	0.01
2	2.49	1.13	0.04	0.02
3	2.50	1.13	0.04	0.02
4	2.49	1.12	0.03	0.02

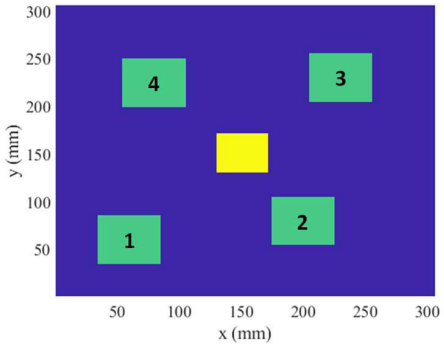

Fig. 4. Map of the sound locations (to scale).

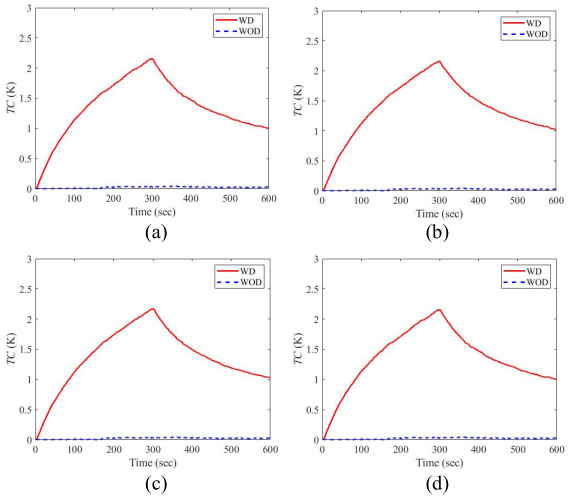

Fig. 5. *TC* for WD and WOD rubber structures for sound locations (a) 1, (b) 2, (c) 3, and (d) 4.

end of the inspection period, or $t = 600$ s) *TC* for the WD and WOD SUTs.

As seen in Fig. 5 and Table II for WD, the temporal behavior of the *TC* is consistent as a function of all the sound locations. For the WOD SUT, there is minimal thermal increase throughout the heating time (also evident in Table II), and the *TC* is effectively equivalent for all the sound locations considered. This minimal thermal increase was expected as the surrounding structure (rubber) in this scenario was intentionally selected due to its low loss factor, particularly when compared with the defect (water). However, when comparing

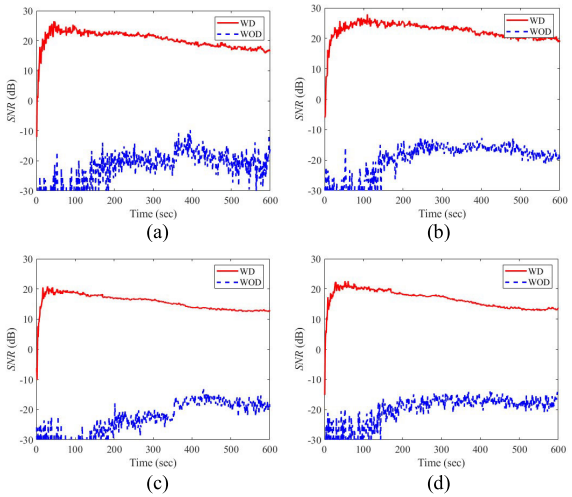

Fig. 6. *SNR* for WD and WOD rubber structures for sound locations (a) 1, (b) 2, (c) 3, and (d) 4.

the *TC* of the WD to that of the WOD, the heat generated from the defect strongly impacts the response, as the *TC* for WD is over an order of magnitude greater than that of the WOD (for all the sound locations). This is expected since the loss factor of the water is substantially higher than that of the rubber structure.

As it relates to the measured *SNR,* seen in Fig. 6, and calculated for all the four sound locations, there is a clear difference between when a defect is present (WD) versus absent (WOD). In addition, for the *SNR* of WD, the defect is considered detectable ($SNR > 0$ [18]) for all the sound locations, whereas this metric is never achieved for the *SNR* of WOD. It should be noted that while there is essentially no difference (for all the sound locations) in the *TC* (Fig. 5) for WD and WOD, there is a difference in *SNR* for each respective sound location (primarily between 0 and 100 s) for WD. For example, the maximum *SNR* achieved per each sound location varies and can be ordered (per sound location) from highest to lowest maximum *SNR* as: 2, 1, 4, and 3. However, each *SNR* still provides detection of the defect for WD (i.e., $SNR > 0$) and does not result in any false positives of $SNR > 0$ for WOD. To this end, for defect heating scenarios, nonuniform heating does not impact *SNR* and the defect remains detectable with arbitrary sound location selection.

As shown in Figs. 5 and 6 and discussed above, the traditional definitions for *TC* and *SNR* [(3) and (4), respectively] can be applied to the defect heating scenario where the structure loss factor is significantly less than that of the defect. However, as most materials are not lossless (or low loss), further examination of the relationship between the structure and defect loss factors and subsequent effect on *TC* and *SNR* is needed. To this end, simulations were conducted in CST Microwave Studio[1] of an SUT as shown in Fig. 3, but with a varying ratio of structure-to-defect dielectric loss factor. The defect cross section in this case is 4 cm × 4 cm and the thickness is 0.0375 cm (with 1 mL of water) and is 0.2 cm from the inspection surface. The structure is 30.5 cm × 30.5 cm with a thickness of 2 cm. The ratio of structure-to-defect loss

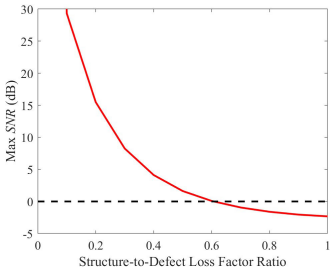

Fig. 7. Maximum calculated *SNR* versus structure-to-defect loss factor ratio.

factor was examined from 0 (no structure loss) to 1 (equal structure and defect loss factors). The defect was assumed to have a constant and substantial dielectric loss factor ($\varepsilon_r'' = 5$), with the loss factor of the structure varying from 0 to 5 to meet the desired range for the ratio of 0–1. It should be noted that when the ratio is greater than 1, the heating scenario is no longer considered to be defect heating, and instead is qualified as structure heating (as a majority of the heat will be induced in the structure in this case). Finally, for reference, the ratio of structure-to-defect loss factors is 0.0056 for the results of Fig. 6. To this end, the maximum calculated *SNR* during the entire inspection period for each structure-to-defect loss factor ratio can be seen in Fig. 7.

As seen in Fig. 7, the threshold of $SNR < 0$ (shown in Fig. 7 as a dashed line) occurs for a ratio of 0.6. Therefore, to achieve defect detection, this ratio must be less than 0.6. For cases that exceed this ratio, use of *SNR* for defect detection is not recommended. It should be noted that if the ratio exceeds 1 (loss factor of the structure is greater than that of the defect, and thus structure heating takes place), the trend of Fig. 7 (maximum *SNR* less than 0) will remain negative. A last point to note is that while the dielectric (versus magnetic) loss factor was considered here, the same results would apply to materials with magnetic loss.

B. Scenario 2: Structure Heating

To illustrate a scenario where structure heating is the primary heat source during an AMT inspection, a four-layer CFRP structure with an absorbing topcoat is considered, as illustrated in Fig. 8. Here, each CFRP layer has a cross section of 30.5 cm × 30.5 cm and a thickness of 0.08 cm. A defect exists in Layer 2 and was manufactured as a centrally located through-hole of diameter 4 cm (also illustrated in Fig. 8). The absorbing topcoat has a cross section of 30.5 cm × 30.5 cm, thickness of 0.22 cm, and approximate $\mu_r = 5 - j10$ (structure-to-defect loss factor ratio of ∞ as the air-type defect is assumed to be lossless). This absorbing topcoat material was specifically chosen for these measurements due to its high magnetic absorption at 2.4 GHz [21], the operating frequency for this measurement. In this way, the topcoat will function as a good absorber of the incident magnetic energy, and hence a strong thermal response will result. As such, the thermal excitation for the CFRP substructure is realized via the topcoat.

As mentioned above, the thermal excitation is directly related to the (spatially nonuniform) incident power density

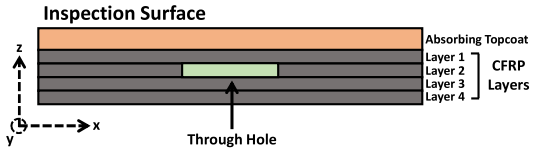

Fig. 8. Illustrative view of a CFRP structure with an absorbing topcoat. The second CFRP layer contains a through-hole defect.

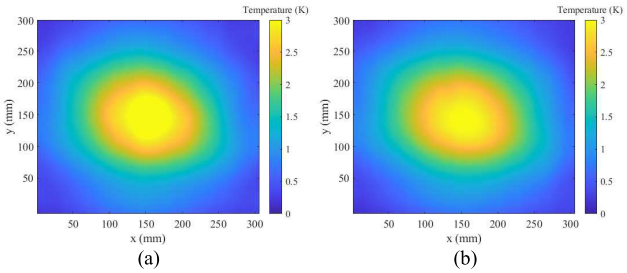

Fig. 9. Thermal surface profile at 90 s for (a) WD and (b) WOD.

TABLE III
MAXIMUM AND FINAL *TC* FOR STRUCTURE HEATING (FIG. 10)

Sound Location	WD		WOD	
	Maximum (K)	Final (K)	Maximum (K)	Final (K)
1	2.49	1.58	1.97	1.34
2	2.15	1.31	1.70	1.13
3	2.12	1.30	1.65	1.10
4	1.93	1.17	1.42	0.91

radiated from the antenna. In such cases where the SUT itself absorbs the incident energy and therefore serves as thermal excitation, the resultant nonuniform heating presents an inherent challenge to the interpretation of results. To illustrate this, measurements were completed using the AMT system described in Fig. 1 on the SUT of Fig. 8 with and without the through-hole defect (i.e., WD and WOD, respectively) with the total number of CFRP layers remaining constant (i.e., always 4). The total inspection time was 180 s, with 90 s each of heating and cooling. The (unprocessed) thermal surface profiles at the end of heating time (i.e., $t = 90$ s) are shown for WD and WOD in Fig. 9.

For WD [Fig. 9(a)], the maximum temperature measured is 0.55 K greater than that of WOD [Fig. 9(b)], but the thermal distribution is effectively equivalent to that of WOD and thus visually masks the presence of the defect. Without additional signal processing (e.g., *TC* and *SNR*) and a reference measurement (i.e., WOD), it is not possible to confidently determine which SUT contains a defect. To further illustrate this issue and using the measured data of Fig. 9, the *TC* and *SNR*, as per (3) and (4), for the WD and WOD SUTs (per each of the four sound locations of Fig. 4) can be seen in Figs. 10 and 11, respectively. In addition, the maximum *TC* and final *TC* (from Fig. 10) are provided in Table III.

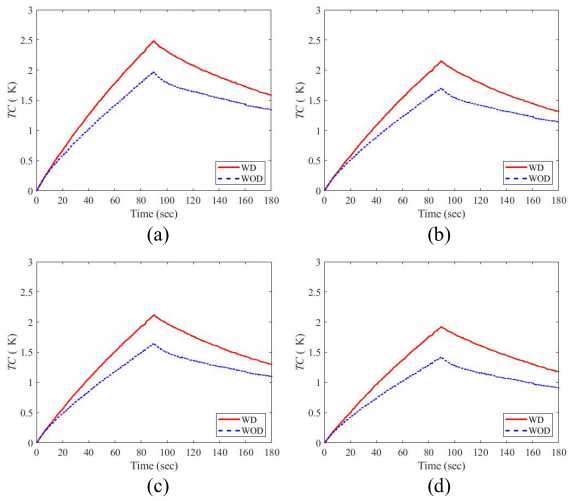

Fig. 10. *TC* for WD and WOD CFRP structures for sound locations (a) 1, (b) 2, (c) 3, and (d) 4.

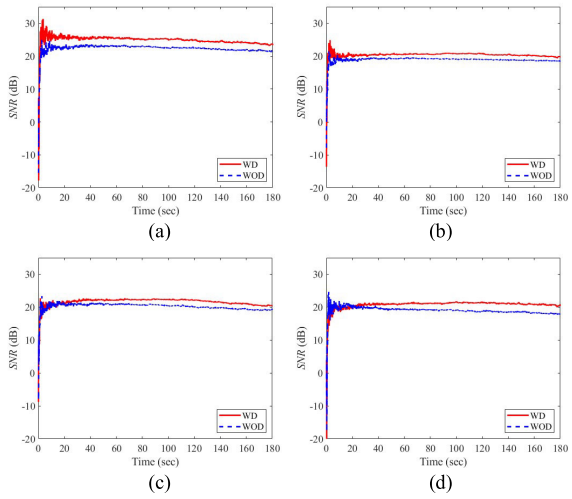

Fig. 11. *SNR* for WD and WOD CFRP structures for sound locations (a) 1, (b) 2, (c) 3, and (d) 4.

From Fig. 10 and Table III, the *TC* of WD and WOD increases with increasing distance between the defect and sound locations (furthest to closest: 1, 3, 4, 2). However, despite these changes, there is no clear indication in the *TC* that a defect is present (for all the four sound locations), as the same temporal behavior manifests for WD and WOD. After approximately 20 s of heating, the *TC* for the WD SUT is greater than that of the WOD SUT (expected as the presence of the defect increases the thermal surface temperature). However, without a reference available (i.e., WOD) for measurement and subsequent analysis and comparison, there is no clear indication of the presence (or lack thereof) of a defect.

In addition, the *SNR* (Fig. 11) does not provide an indication of the defect (for all the four sounds locations), as the results for WD and WOD are similar (both in magnitude and temporal behavior). Moreover, the metric for detectability of $SNR > 0$ [18] is also met when a defect is not present. In the case of WOD, this creates a false positive for defect detection and is due to nonuniform structure heating (seen in Fig. 9). To this

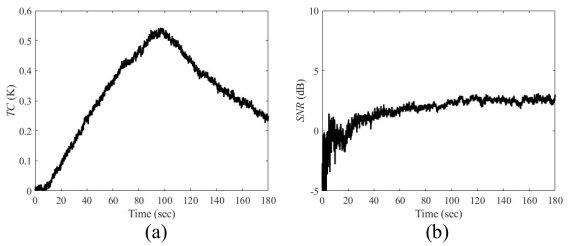

Fig. 12. (a) *TC* and (b) *SNR* for CFRP structures when using WOD SUT as a reference.

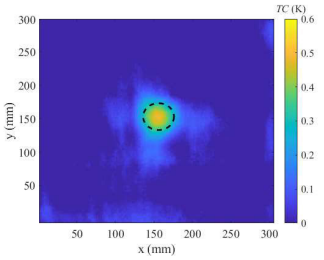

Fig. 13. Thermal surface profile of *TC* for WD at 90 s of heating using WOD as a reference.

end, as both *TC* and *SNR* do not facilitate reliable detection for cases of nonuniform structure heating, a new detection metric is needed that is sensitive to the presence of a defect for such cases.

To overcome this challenge of ambiguity in defect detection, one solution may be to incorporate a reference measurement (from a known WOD SUT) into the calculation of *TC* and *SNR*. In this way, the sound parameters used to calculate *TC* and *SNR* [i.e., μ_S and σ_S in (3) and (4)] can be determined from this second (independent reference) measurement. Using this approach, *TC* and *SNR* for the CFRP structure are shown in Fig. 12. From Fig. 12(a), it can be observed that using the WOD SUT as a reference, the presence of a defect can be observed in the finite response of the *TC*, as the *TC* will inherently be zero otherwise. In addition, using a reference SUT (WOD), the thermal sensitivity of the camera (30 mK in this work) can be considered a threshold for defect detection in the *TC*. The *TC* is further illustrated in Fig. 13, where the surface profile of *TC* for WD is shown. Here, the presence of a defect is clearly evident (indicated by the dashed black line). Similarly, as seen in Fig. 12(b), the metric of $SNR > 0$ can be used for defect detectability since a reference (WOD) has been used. If no defect is present, the *SNR* will approach $-\infty$ [per (4)].

While the use of a reference SUT (WOD) does facilitate clear defect detection (e.g., directly through *TC* and when $SNR > 0$), the practicality of a required reference SUT is limiting. In other words, the availability of representative defect-free SUT is unlikely for real-world inspection needs. To this end, a reformulation of *SNR* is considered, as aspects of this quantity may be modified to rely solely on the thermal response of the WD SUT [e.g., change σ_S to σ_D in (4)] for calculation of *SNR*. However, per the definition of *TC*, modification to remove the necessity of sound measurement

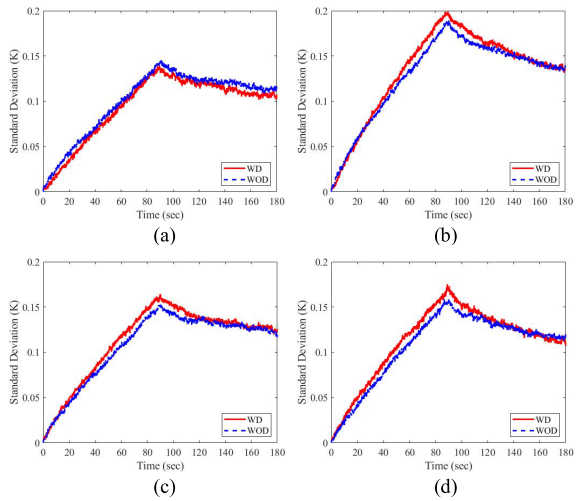

Fig. 14. Standard deviation, σ_S, of ΔT for sound locations (a) 1, (b) 2, (c) 3, and (d) 4 over the inspection time.

cannot be completed as any changes to (3) (i.e., T_S to T_D) will result in $TC = 0$.

IV. Reformulation of *SNR*

A. Scenario 2: Structure Heating

As mentioned previously, when (4) (*SNR*) is applied to the results of an AMT inspection that features structure heating (i.e., Fig. 8), *SNR* does not serve as a clear indicator for defect detection with a single measurement due to nonuniform surface heating. To this end, a reformulation of *SNR* for thermographic inspections with nonuniform thermal heating (including AMT) is necessary to facilitate practical inspections (without the need of a reference measurement). As it relates to the definition of *SNR*, there are three parameters that can be considered [see (4)]: μ_D (mean surface temperature at defect location), μ_S (mean surface temperature at sound location), and σ_S (standard deviation at sound location). The value of μ_D is fixed (for a given inspection), as this is the mean surface temperature at the defect location. In addition, the effect of μ_S was investigated in Section III by applying measurements from various sound locations (sound locations 1–4 in the WD SUT) across an inspection surface. In other words and as seen in Fig. 11, the change in μ_S did not impact the detectability of the defect as there is no notable difference in Fig. 11(a)–(d). Moreover, despite the differences in μ_S for different sound locations (evident in the maximum *TC* in Table III), the standard deviation (σ_S) at each sound location for the WD and WOD SUTs does not exhibit this same behavior, as is shown in Fig. 14. As seen, σ_S is effectively equivalent for all the four sound locations for WD and WOD and therefore does not depend on the presence of a defect.

To this end, to be effective for nonuniform heating, the modified formulation of *SNR* (4) must include a parameter that is sensitive to the presence of a defect, as σ_S (Fig. 14) is not. Therefore, the dependency of *SNR* to the presence of a defect is solely attributed to μ_D, as is illustrated in Fig. 15, where σ_D for WD and WOD is shown. As seen in Fig. 15(a) (σ_D for WD), there is a notable temporal change when

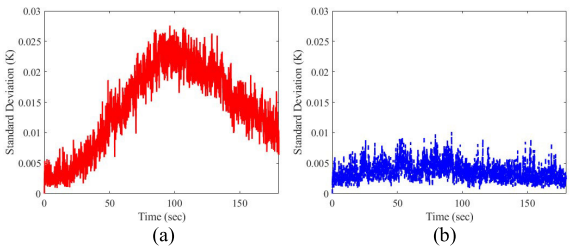

Fig. 15. Standard deviation of the defect location, σ_D, of (a) WD and (b) WOD over the inspection time at sound location 1.

compared with Fig. 15(b) (σ_D for WOD). In other words, the standard deviation of the surface temperature at a location varies when a defect is present. As such, this quantity, σ_D, may be used in place of σ_S in the definition of *SNR* to improve the sensitivity of *SNR* to the presence of a defect and provide an indication of the same. Therefore, a modified definition of *SNR*, denoted as SNR_r, is proposed as

$$SNR_r(t) = 20\log_{10}\frac{|\mu_D(t) - \mu_S(t)|}{\sigma_D(t)}. \tag{7}$$

Using (7), SNR_r was calculated using previous measurements for the WD and WOD SUTs (Fig. 8) and is shown in Fig. 16. As seen, there is a distinction between SNR_r of WD and WOD for all the four sound locations. This distinction begins at approximately 25 s, where σ_D deviates from σ_S (see Fig. 15) and remains for the duration of the inspection period. To this end, to explain the differences between WD and WOD, the cooling period is analyzed. During this period, WD exhibits a zero slope and then increases (positive slope) while WOD is asymptotic. This difference in WD and WOD is attributed to σ_D, which is affected by the presence of a defect (as shown in Fig. 15) and accounts for defect altering the flow of heat. This distinction in SNR_r between WD and WOD for structure heating scenarios was not previously possible [using *SNR* of (4)], as WD and WOD were essentially equivalent (see Fig. 11). To address the differences in SNR_r, the variance over the cooling time was calculated to quantify the temporal noise (in Fig. 16) and is seen in Table IV. As seen, the difference in variance between WD and WOD for SNR_r is substantial (50 times greater) than that of *SNR*. To this end, it is no longer the magnitude of SNR_r (e.g., $SNR > 0$) that determines the detectability of a defect, but the reduction in temporal noise (quantified by the variance of SNR_r over the cooling period).

To further illustrate the improvement in signal processing provided by SNR_r, the same is shown across the inspection surface and can be seen in Fig. 17, with the black dashed line indicating the defect location. From Fig. 17, there is a clear indication (evidenced by spatial variation in variance) of the presence of a defect [Fig. 17(a)] and when a defect is absent [Fig. 17(b)]. This indication is due to a reduction in temporal variance across the profile during the cooling period when a defect is present. Finally, while Fig. 13 (*TC* using a reference measurement) provided a precise indication of the defect location, using SNR_r is advantageous as a reference measurement is not needed and the presence of the defect can still be determined, but does not provide a precise location.

TABLE IV
VARIANCE DURING THE COOLING PERIOD OF *SNR* AND *SNRr* FOR STRUCTURE HEATING (FIGS. 11 AND 16)

Sound Location	*SNR* Variance (dB^2)		SNR_r Variance (dB^2)	
	WD	WOD	WD	WOD
1	0.29	0.15	2.86	13.20
2	0.12	0.04	2.59	13.15
3	0.45	0.26	2.59	13.14
4	0.09	0.13	2.56	13.07

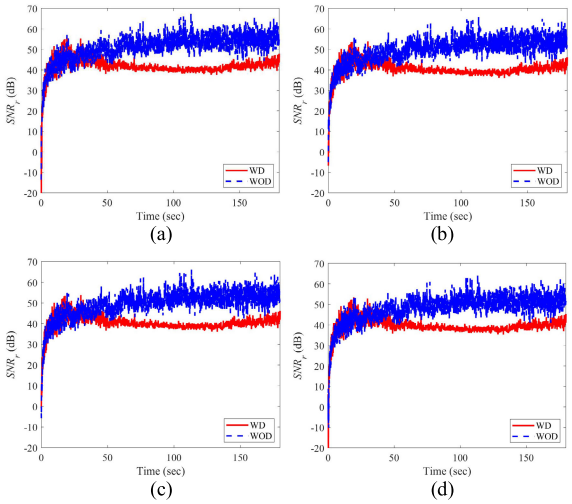

Fig. 16. SNR_r for WD and WOD CFRP structures for sound locations (a) 1, (b) 2, (c) 3, and (d) 4.

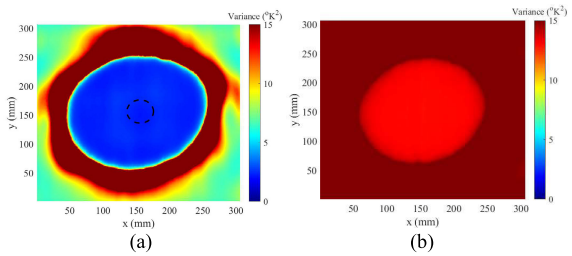

Fig. 17. Calculated average variance of SNR_r over the cooling time for (a) WD and (b) WOD CFRP structures at sound location 1.

B. Scenario 1: Defect Heating

As the modification of *SNR* (e.g., SNR_r) has improved detection for structure heating scenarios, its application to defect heating needs to be examined as well. To this end, SNR_r (7) for the defect heating results of Fig. 3 is shown in Fig. 18 (for the four sound locations), with the variance of SNR_r during the cooling period provided in Table V. As seen, there is a distinct difference in SNR_r of the WD and WOD SUTs throughout the inspection period. More specifically, while SNR_r for WD remains relatively constant during the cooling period, the SNR_r for WOD has more temporal variation during the cooling period when compared with WD. In addition, the metric of $SNR = 0$ for detectability remains a viable metric for defect detection, as the response (in all the cases) for WOD does not exceed 0 dB consistently (rather, sporadically due to

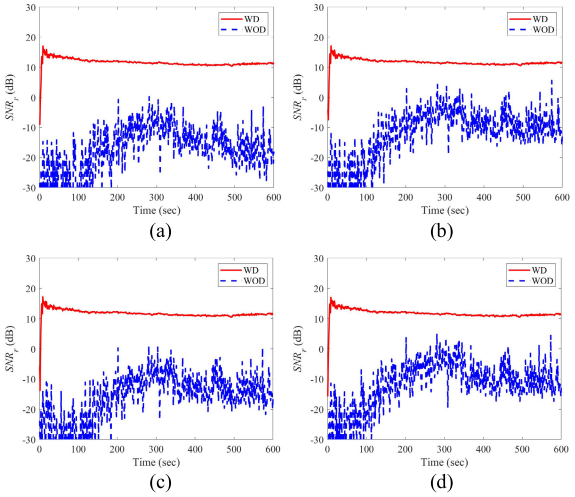

Fig. 18. SNR_r for WD and WOD rubber structures for sound locations (a) 1, (b) 2, (c) 3, and (d) 4.

TABLE V
VARIANCE DURING THE COOLING PERIOD OF *SNR* AND *SNRr* FOR DEFECT HEATING (FIG. 18)

Sound Location	SNR_r Variance (dB^2)	
	WD	WOD
1	0.06	26.64
2	0.06	19.55
3	0.07	20.71
4	0.06	21.93

noise). In addition, the results of Table V also support the use of SNR_r, as the minimum variance occurs for the WD SUT (as above for structure heating), and thus removes the reliance of using the metric of $SNR > 0$. In this way, a single metric for detectability can be considered, regardless of the heating scenario. In addition, SNR_r for WD indicates that the results are independent of a sound location as the variance over the cooling period is consistent among each location considered. A final note is that while *SNR* requires the consideration of the structure-to-defect loss factor ratio, SNR_r does not require this consideration and instead works on the full range of the ratio (0 to ∞). This is confirmed through the two scenarios considered in this work, where scenario 1 (defect heating) considered a ratio of 0.0056 (i.e., near 0) and scenario 2 (structure heating) considered a ratio of ∞ (i.e., defect has a loss factor of 0). Thus, both ends of the ratio range were examined in this work for *SNR* and SNR_r, where *SNR* had a limitation of usability at a ratio of 0.6.

V. CONCLUSION

AMT is a coupled electromagnetic and thermographic NDT&E technique that has seen success in recent years in the civil and aerospace industries, among others. The thermal excitation is achieved through an active electromagnetic source (a radiating antenna) with subsequent electromagnetic absorption by a defect or structure of an SUT. As a result of the

radiating electromagnetic energy serving as the thermal excitation, the induced heat is spatially nonuniform. To this end, this work challenges the use of the traditional thermographic postprocessing techniques, thermal contrast (*TC*) and *SNR*, for the two fundamental heating scenarios of AMT (defect and structure heating). For defect heating, it was found that the nonuniform thermal excitation did not impact the use of *TC* and *SNR* for defect detection. More specifically, for the SUT without a defect (WOD), *SNR* never exceeds 0 dB. Conversely, *SNR* for the SUT with a defect (WD) is greater than 0 dB after a few seconds.

For the other considered scenario, structure heating, it was found that the traditional definitions of *TC* and *SNR* were not applicable when using a single measurement (i.e., no reference measurement). The *SNR* values for WOD and WD exceed 0 dB at the same time and do not provide a notable difference between the two SUTs. To this end, a reformulated *SNR* definition (referred to as SNR_r) was proposed and implemented. For structure heating, SNR_r provided a clear indication of the presence of a defect without the need of a reference measurement (which *SNR* required). When observing the variance of SNR_r over the cooling period, the variance for WD and WOD is, on average, 2.65 and 13.14 dB^2, respectively (variance difference of 9 dB^2). In addition, SNR_r was also successfully applied to the defect heating scenario. In this scenario, the variance of SNR_r over the cooling period for WD and WOD is 0.06 and 22.21 dB^2, respectively (variance difference of 22 dB^2). Thus, SNR_r can be used in both the fundamental AMT heating scenarios and becomes a viable and recommended alternative the o traditional *SNR* for all types of nonuniform thermal excitation, such as AMT. In future works, this modified *SNR* (SNR_r) will be considered for application to other thermographic techniques (such as that using a traditional heat lamp excitation). In addition, the potential to remove the a priori requirement of known defect and sound locations will be considered.

REFERENCES

[1] D. Donskoy, A. Sutin, and A. Ekimov, "Nonlinear acoustic interaction on contact interfaces and its use for nondestructive testing," *NDT E Int.*, vol. 34, no. 4, pp. 231–238, Jun. 2001.

[2] G. Y. Tian, A. Sophian, D. Taylor, and J. Rudlin, "Multiple sensors on pulsed eddy-current detection for 3-D subsurface crack assessment," *IEEE Sensors J.*, vol. 5, no. 1, pp. 90–96, Feb. 2005.

[3] X. P. Maldague, *Theory and Practice of Infrared Technology for Nondestructive Testing*. New York, NY, USA: Wiley, 2001.

[4] R. Zoughi, *Microwave Non-Destructive Test and Evaulation Principles*, vol. 4. Dordrecht, The Netherlands: Kluwer, 2000.

[5] Y.-K. An, J. M. Kim, and H. Sohn, "Laser lock-in thermography for detection of surface-breaking fatigue cracks on uncoated steel structures," *NDT E Int.*, vol. 65, pp. 54–63, Jul. 2014.

[6] S. D. Holland et al., "Quantifying the vibrothermographic effect," *NDT E Int.*, vol. 44, no. 4, pp. 775–782, 2011.

[7] H. Zhang, R. Yang, Y. He, A. Foudazi, L. Cheng, and G. Tian, "A review of microwave thermography nondestructive testing and evaluation," *Sensors*, vol. 17, no. 5, p. 1123, May 2017.

[8] A. Mirala, M. T. A. Qaseer, and K. M. Donnell, "Health monitoring of RAM-coated structures by active microwave thermography," *IEEE Trans. Instrum. Meas.*, vol. 70, pp. 1–11, 2021.

[9] A. Foudazi, C. A. Edwards, M. T. Ghasr, and K. M. Donnell, "Active microwave thermography for defect detection of CFRP-strengthened cement-based materials," *IEEE Trans. Instrum. Meas.*, vol. 65, no. 11, pp. 2612–2620, Nov. 2016.

[10] A. Mirala, A. Foudazi, M. T. A. Qaseer, and K. M. Donnell, "Active microwave thermography to detect and locate water ingress," *IEEE Trans. Instrum. Meas.*, vol. 69, no. 12, pp. 9774–9783, Dec. 2020.

[11] H. He et al., "Detection of debonding defects between radar absorbing material and CFRP substrate by microwave thermography," *IEEE Sensors J.*, vol. 22, no. 5, pp. 4378–4385, Mar. 2022.

[12] S. Shepard, "Flash thermography of aerospace composites," in *Proc. PAN-Amer. Conf. Nondestruct. Test.*, Oct. 2007, pp. 1–7.

[13] J. Sun, W. Wang, and Q. Yue, "Review on microwave-matter interaction fundamentals and efficient microwave-associated heating strategies," *Materials*, vol. 9, no. 4, p. 231, Mar. 2016.

[14] J. H. Lienhard and J. H. Lienhard, *A Heat Transfer Textbook*, 4th ed. Cambridge, MA, USA: Philogiston, 2017.

[15] C. Ibarra-Castanedo et al., "Comparative study of active thermography techniques for the nondestructive evaluation of honeycomb structures," *Res. Nondestruct. Eval.*, vol. 20, no. 1, pp. 1–31, Jan. 2009.

[16] C. Maierhofer et al., "Evaluation of different techniques of active thermography for quantification of artificial defects in fiber-reinforced composites using thermal and phase contrast data analysis," *Int. J. Thermophys.*, vol. 39, no. 5, pp. 1–37, Mar. 2018.

[17] E. D'Accardi et al., "Pulsed phase thermography approach for the characterization of delaminations in CFRP and comparison to phased array ultrasonic testing," *J. Nondestruct. Eval.*, vol. 38, no. 1, pp. 1–37, Jan. 2019.

[18] K. Srinivas, A. O. Siddiqui, and J. Lahiri, "Thermographic inspection of composite materials," in *Proc. Nat. Seminar Non-Destruct. Eval.*, vol. 12, 2006, pp. 7–9.

[19] M. Kempin, M. T. Ghasr, J. T. Case, and R. Zoughi, "Modified waveguide flange for evaluation of stratified composites," *IEEE Trans. Instrum. Meas.*, vol. 63, no. 6, pp. 1524–1534, Jun. 2014.

[20] U. Kaatze, "Complex permittivity of water as a function of frequency and temperature," *J. Chem. Eng. Data*, vol. 34, no. 4, pp. 371–374, Oct. 1989.

[21] *Cuming Microwave, C-RAM FF-2 Technical Bulletin*. Accessed: Dec. 2023. [Online]. Available: https://www.cumingmicrowave.com/pdf/310-Rubber%20Sheets/310-7%20C-RAM%20FF-2.pdf

Logan M. Wilcox (Graduate Student Member, IEEE) was born in Norfolk, VA, USA, in 1996. He received the B.S. degree in computer engineering from the Missouri University of Science and Technology (Missouri S&T), Rolla, MO, USA, in 2020, where he is currently pursuing the Ph.D. degree in electrical engineering.

Currently, he is a Graduate Research Assistant with the Microwave Sensing (μSense) Laboratory, Missouri S&T. His research interests include nondestructive testing and evaluation, microwave and thermal material characterization, and thermal image analysis and processing.

Mr. Wilcox is in the inaugural class of the Kummer Innovation and Entrepreneurship Doctoral Fellowship Program at Missouri S&T. In addition, he was a recipient of the IEEE Instrumentation and Measurement (I^2MTC) Graduate Fellowship in 2020 and the IEEE I^2MTC Student Travel Grant in 2022.

Kristen M. Donnell (Senior Member, IEEE) received the B.S.E.E. degree from Colorado State University, Fort Collins, CO, USA, in May 2001, the M.S.E.E. degree from the University of Missouri-Rolla, Rolla, MO, USA, in December 2003, and the Ph.D. degree in electrical engineering from the Missouri University of Science and Technology (Missouri S&T), Rolla, in December 2010.

Prior to starting the Ph.D. work, she was employed by Raytheon Company, Tewksbury, MA, USA, from 2003 to 2006, as a Systems Engineer and an Electrical Engineer. She is currently a Woodard Associate Professor of Excellence with the Department of Electrical and Computer Engineering, Missouri S&T, and the Director of the Microwave Sensing (μSense) Laboratory, Rolla. Her current research interests include thermography, frequency-selective surfaces, materials' characterization, and microwave and millimeter-wave nondestructive testing.

Dr. Donnell has been involved with the IEEE Instrumentation and Measurement Society since 2007. She currently serves as the Vice President for the Finance Committee and the Chair for the Distinguished Lecturer Program.